Understanding IFRA for Detecting Synchronous Machine Winding Short Circuit Faults Based on Image Classification and Smooth Grad-CAM++

Yu Chen, Zhongyong Zhao, *Member, IEEE*, Yueqiang Yu, Wei Wang, and Chao Tang, *Member, IEEE*

***Abstract*—Fault diagnosis of the synchronous machine is essential for the safe operation of the modern power system. Recently, impulse frequency response analysis (IFRA) has been used to detect synchronous machine winding short circuit (SC) faults since the failure will significantly alter the IFRA signature of machines. However, there is no standard and reliable code for interpreting the IFRA signatures. It often refers to the frequency response analysis of power transformer standards, the mathematical-statistical indicator of relative factor is directly used to perform the judgment by the standards' threshold, which might not be appropriate. Besides, the internal mechanism of frequency response analysis diagnosis is unclear. Therefore, this study proposes a technique based on image classification and smooth grade and gradient-based class activation maps (Smooth Grad-CAM++) to understand and interpret the IFRA method. It trains and analyzes the visualization results of the fault data set of a 5 kW synchronous machine's winding. The experimental results show that the average accuracy of the image classification model based on Resnet18 reaches 99.63%. We performed an IFRA difference analysis according to the visualization results and gave some suggestions about IFRA. The training and detection process can be accelerated based on these suggestions. To illustrate the generalization of the suggestions, another 8 kW synchronous machine is used for the case study, and the experimental results show that these suggestions are still effective. The main contributions of this study are understanding the internal mechanism of IFRA diagnosis from another perspective and providing some conclusions different from previous research results on the IFRA method for the synchronous machine.**

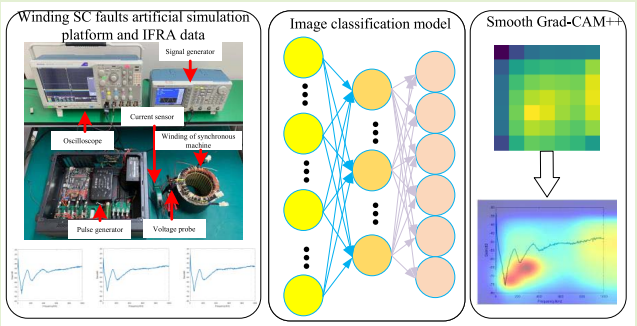

***Index Terms*— Fault detection, image classification model, impulse frequency response analysis (IFRA), smooth grade and gradient-based class activation maps (Smooth Grad-CAM++), synchronous machine, winding.**

Manuscript received 19 October 2022; accepted 22 November 2022. Date of publication 15 December 2022; date of current version 31 January 2023. This work was supported in part by the Fundamental Research Funds for the Central Universities under Grant SWU-KT22027, in part by the National Natural Science Foundation of China under Grant 51807166, in part by the Venture and Innovation Support Program for Chongqing Overseas Returnees under Grant cx2019123, and in part by the Natural Science Foundation of Chongqing under Grant cstc2019jcyj-msxmX0236. The associate editor coordinating the review of this article and approving it for publication was Dr. Peng Wang. *(Corresponding author: Zhongyong Zhao.)*

Yu Chen is with the College of Engineering and Technology, Southwest University, Chongqing 400716, China, and also with the School of Electrical and Electronic Engineering, Huazhong University of Science and Technology, Wuhan 430074, China (e-mail: cy1034429543@email.swu.edu.cn).

Zhongyong Zhao, Yueqiang Yu, and Chao Tang are with the College of Engineering and Technology, Southwest University, Chongqing 400716, China (e-mail: zhaozy1988@swu.edu.cn; yyq14011@email.swu.edu.cn; swutc@swu.edu.cn).

Wei Wang is with the School of Electrical and Electronic Engineering, Huazhong University of Science and Technology, Wuhan 430074, China (e-mail: husterww@hust.edu.cn).

Digital Object Identifier 10.1109/JSEN.2022.3225210

I. Introduction

SYNCHRONOUS machines are widely used in power plants, aerospace, aviation, and other fields [1], [2]. At the same time, as one of the essential components of the power system, the large synchronous machine completes the conversion from mechanical energy to electrical energy. In various electric energy generation methods, 90% of electric energy is provided by synchronous machines in hydropower plants or thermal power plants [3]. Synchronous machines have complex structures and diverse operating environments. Various electromagnetic, mechanical, and thermal stresses could significantly impact the components of devices. Thus, the machines could be defective. Relevant reference [4] shows many kinds of faults in large synchronous machines, of which 66% are winding faults. Among them, the winding interturn and ground short circuit (SC) faults are very common. If the synchronous machines with SC faults are not handled in time, it may damage the devices and even lead to power

system collapse and casualties. Accurately detecting winding SC faults can ensure large synchronous machines' safe and reliable operation.

Many methods have emerged to detect winding SC faults in recent years, including online and offline detection methods. Many researchers use ac impedance, dielectric dissipation, dc resistance, and the open transformer method to detect the winding SC faults when the machine is out of service [5], [6], [7]. The online techniques include the stator parallel branch circulation method, vibration monitoring of stator and rotor method, temperature field variation method, etc. [8], [9], [10]. In addition, many scholars are concerned about the real-time change of winding state and use field circuit coupling simulation, such as establishing a temperature field to analyze synchronous machines' winding faults [10]. These works are significant to the detection of machine winding faults.

In particular, some researchers use frequency response analysis (FRA), which has been widely used in power transformer winding mechanical fault detection, to detect synchronous machine winding faults [11], [12]. Besides, impulse FRA (IFRA) has also been introduced [11]. IFRA has the advantage as same as FRA. Compared with FRA using frequency sweep to obtain the frequency response curve, IFRA provides an alternative to serving the same objective. It obtains the frequency response curve by a high-frequency (HF) impulse signal. Furthermore, IFRA has the advantages of high detection sensitivity, fast detection speed, and good economy [13], [14], [15], [16].

Whether FRA or IFRA, the interpretation of frequency response signature matters. There are two main methods.

1) Construct and calculate various mathematical and statistical indicators, including the indicators related to all frequency points and the indicators related to resonance and antiresonance. This mathematical indicator-based method has been most widely used.
2) The advanced artificial intelligence (AI) method also provides an alternative interpretation in which machine learning classifiers could be used to detect the types, extents, and locations of faults.

In the first method, Zhao et al. [12] analyze the influence of winding interturn SC fault on FRA by establishing a gray box model. It investigates the influence of faults on each resonant point and then diagnoses the fault. The impact of stator core on FRA is studied in [17] to verify the effectiveness of detecting winding defects by the FRA method. Some researchers analyze the relationship between winding faults and FRA curves and provide a series of mathematical and statistical indicators positively correlated with the fault degree [18].

In the second method, the indicators are often used for fault classification by machine learning. Liu et al. [19] use the support vector machine for winding fault classification based on particle swarm optimization (SVM-PSO). Liu et al. [20] also classify winding faults based on polar plots and multiple SVM. Chen et al. [11] provide an anomaly detection method named isolation forest (IF) to distinguish normal and fault windings through unsupervised learning. In addition, although the method of fault detection is not necessarily the frequency responses, many researchers use advanced deep learning methods to detect the faults, such as convolutional neural network (CNN), recurrent neural network (RNN), and other network structures [21].

So far, there is, however, no standard and reliable interpretation code of frequency response. The current technique still has the following defects.

1) For the mathematical indicator-based methods, the structure of the synchronous machine is diverse from that of the power transformer. The current diagnosis of synchronous machines, however, refers to the standard of frequency response analysis of power transformers [12], which could be unreasonable. For instance, the division of frequency band, namely, 1–100, 100–600, and 600–1000 kHz, stands for low-frequency (LF), middle-frequency (MF), and HF bands, respectively, which might be unsuitable for the synchronous machine.
2) For the AI-based interpretation method, the common problem is that the machine learning model is a black-box model and cannot intuitively provide a detection standard. Besides, there is no appropriate method to reasonably explain and prove the detection process. Relevant researchers cannot peep into the internal diagnosis mechanism of the model and are not sure whether these models work according to the requirements.

Since deep learning has been widely applied to various tasks with good performance, people have marveled at its effectiveness while questioning its black box [22], [23], [24], [25]. As the AI intelligence community grows, there is a growing interest in how the model works, i.e., using the interpretability method to explain its black box [23]. Understanding how models work can guide engineers in feature engineering, direct data collecting, decisions making, and building trust between models and people [24], [25]. In the fault diagnosis community, there are relatively few works at present. Yang et al. [26] intuitively observed the discriminative features of different rolling bearing health conditions based on the neuron activation maximization and the saliency map methods. Fan et al. [27] use an attention mechanism to understand fault signal characteristics of centrifugal fans from different scales and dimensions. Currently, there is no relevant work to use the interpretability model to understand IFRA for the fault diagnosis of synchronous machine windings.

In this context, this study combines the image classification model and the interpretability model Smooth Grad-CAM++ to visualize, analyze, and understand the mechanism of IFRA for detecting synchronous machine winding SC faults. Perhaps this study can conclude differently from previous studies, which have been proven and confirmed in the experimental test. The main contributions of this study are as follows.

1) For the first time, the interpretability technique of deep learning is combined with IFRA to understand synchronous machine winding SC faults.
2) This study first detects synchronous machine winding SC faults based on image classification and frequency response curves.
3) We combine previous standards to propose some suggestions that are more sensitive and effective for

winding SC faults diagnosis of synchronous machines, which could have strong engineering implications.

The remainder of this study is organized as follows. The principles of IFRA and Smooth Grad-CAM++ are briefly introduced in Section II. The artificial fault experiment of winding SC faults is presented in Section III. An image classification model based on Resnet is established to detect winding SC faults and compared with other image classification models in Section IV. The mechanism of IFRA is analyzed according to the visualization results of Smooth Grad-CAM++ in Section V. Section VI introduces a case study. Some discussions are in Section VII. Finally, the conclusions and suggestions are provided in Section VIII.

II. Brief Introduction of Corresponding Methods

A. Theory of IFRA

Recently, researchers have achieved good results by using IFRA to extract the winding faults characteristics of power transformers [17], [18], [19]. Windings of synchronous machines and power transformers have similar components. Thus, the IFRA technique could be transferred to detect synchronous machine winding faults [11], [12]. The essence of IFRA is that under the action of an HF impulse signal $V_{\text{in}}(k)$, the stator winding of each slot can be regarded as a two-port network composed of inductance, capacitance, and resistance. Its transfer function $H(k)$, is determined accordingly for a certain synchronous machine. When the winding of the synchronous machine has an interturn or ground SC fault, the parameters of its equivalent circuit model will change; that is, the transfer function will change. Transfer function $H(k)$ can be obtained according to the input $V_{\text{in}}(k)$ and output $I_{\text{out}}(k)$. Similarly, the output can also use the response voltage

$$V_{\text{in}}(k) = \sum_{n=0}^{N-1} v_{\text{in}}(n)\, e^{-j\frac{2\pi}{N}\text{kn}} \tag{1}$$

$$I_{\text{out}}(k) = \sum_{n=0}^{N-1} i_{\text{out}}(n)\, e^{-j\frac{2\pi}{N}\text{kn}} \tag{2}$$

$$H(k) = 20\log_{10}\frac{|I_{\text{out}}(k)|}{|V_{\text{in}}(k)|} \tag{3}$$

where $v_{\text{in}}(n)$ and $i_{\text{out}}(n)$ are the N points sampling signal of impulse voltage and response current; $V_{\text{in}}(k)$ and $I_{\text{out}}(k)$ are fast Fourier transforms (FFTs) of $v_{\text{in}}(n)$ and $i_{\text{out}}(n)$; $H(k)$ is the transfer function.

B. Theory of Smooth Grad-CAM++

To explain how deep learning works, researchers proposed a visualization method named class activation map (CAM) without training [28]. Then an improved method called Smooth Grad-CAM++ was proposed [29], and its frame diagram is shown in Fig. 1.

Generally, CAM uses the gradient of Y^c to reflect the influence of the feature map on each element of the last layer of CNN

$$\frac{\partial Y^c}{\partial A_{i,j}^K} \tag{4}$$

where c represents the predicted label, Y is the output, K represents the Kth convolution kernel in the convolution layer, and $(i,\ j)$ represents the values of row i and column j of the convolution kernel; A is the output of the convolution layer, as shown in Fig. 1.

Compared with the CAM, Smooth Grad-CAM++ adds Gaussian noise to the original input, a simple way to improve gradient sensitivity

$$M_c^n(x) = Y_c\left(x + N\left(0, \sigma^2\right)\right) \tag{5}$$

$$D_{1,n}^{K(i,j),c}(x) = \frac{\partial M_c^n(x)}{\partial A_{i,j}^K} \tag{6}$$

$$D_{2,n}^{K(i,j),c}(x) = \frac{\partial^2 M_c^n(x)}{\partial^2 A_{i,j}^K} \tag{7}$$

$$D_{3,n}^{K(i,j),c}(x) = \frac{\partial^3 M_c^n(x)}{\partial^2 A_{i,j}^K} \tag{8}$$

where $D_{1,n}^{K(i,j),c}(x)$ represents the first-order partial derivatives of location $(i,\ j)$ of the nth sample of kth convolution kernel of the convolution layer, the predicted label of which is c, added with Gaussian noise $N(0, \sigma^2)$, the mean is 0, and default standard deviation is usually 0.15. The same rule can be adapted to $D_{2,n}^{K(i,j),c}(x)$ and $D_{3,n}^{K(i,j),c}(x)$, which are second and third-order partial derivatives, respectively.

$a_c^{K(i,j)}$ captures the importance of location $(i,\ j)$ for activation map $A_{i,j}^K$ for label c (9), shown at the bottom of the page.

W_k^c captures the importance of a particular activation map $A_{i,j}^K$ by

$$W_k^c = \sum_{i=1}^{I}\sum_{j=1}^{J} a_c^{K(i,j)}\text{Relu}\left(\frac{1}{N}\sum_{n=1}^{N} D_{1,n}^{K(i,j),c}\right). \tag{10}$$

$L_{i,j}^c$ captures the important location of classification

$$L_{i,j}^c = \text{Relu}\left(\sum_{k=1}^{K} W_c^{k(i,j)} A_{i,j}^k\right). \tag{11}$$

Then, $L_{i,j}^c$ is visualized as the heat map in Fig. 1. The visualization result process, combined $L_{i,j}^c$ with the actual picture input, is shown in Fig. 2.

III. Artificial Fault Experiment of Winding SC Faults

A. Introduction of the Winding SC Faults Artificial Simulation Platform

IFRA measurement is carried out on a 5 kW, three-phase, salient pole synchronous machine winding (without

$$a_c^{K(i,j)} = \frac{\frac{1}{N}\sum_{n=1}^{N} D_{1,n}^{K(i,j),c}}{\frac{2}{N}\sum_{n=1}^{N} D_{2,n}^{K(i,j),c} + \sum_{i=1}^{I}\sum_{j=1}^{J} A_{i,j}^K \frac{1}{N}\sum_{n=1}^{N} D_{3,n}^{K(i,j),c}} \tag{9}$$

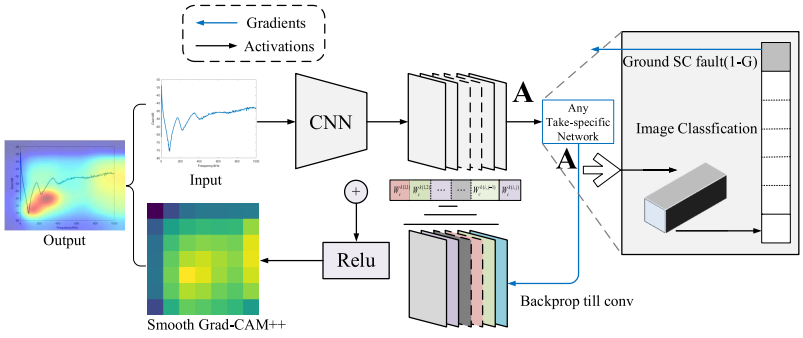

Fig. 1. Frame diagram of smooth grad-CAM++.

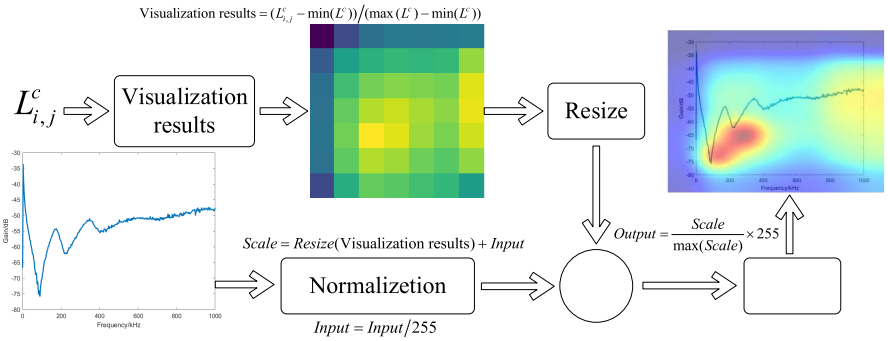

Fig. 2. Visualization result processing process ($L^c_{i,j}$ is output based on Smooth Grad-CAM++; input is the red, green and blue (RGB) value of IFRA curve image; resize is to fill the heatmap to the same size as the input).

TABLE I
NAMEPLATE VALUES OF SYNCHRONOUS MACHINE

Characteristics	Parameter value
Rated power	5kW
Rated voltage	380V
Frequency	50Hz
Pole pairs	1
Number of slots	36
Rated speed	1500rpm

rotor). The nameplate of the synchronous machine is shown in Table I. Fig. 3(a) shows the actual experimental wiring diagram, and Fig. 3(b) shows the measurement wiring diagram. The winding SC faults artificial simulation platform comprises a homemade pulse generator (pulse amplitude of 0–4 kV, the leading edge time is within 40 ns, and the pulsewidth is adjusted in 10–1000 ns), a current sensor (model: 150, Pearson, bandwidth: 40 Hz–20 MHz, sensitivity: 0.5 V/A), a voltage probe (model: P5100A, Tektronix, bandwidth: 500 MHz), and an oscilloscope (model: MDO4104C, Tektronix, bandwidth: 1 GHz). In Fig. 3, the excitation voltage and response current are measured using a voltage probe and a current sensor. An oscilloscope records the waveform. Many IFRA tests are carried out under the same state.

The excitation and response signals of 64 measurements are averaged to reduce the impact of white noise on the measurement. The pulse amplitude is 480 V, the pulsewidth is less than 700 ns, the rising time is less than 50 ns, and the pulse waveform is shown in Fig. 4. The sampling rate is 25 MHz, and the sampling point is 10 k. Finally, the average time-domain signal is used for IFRA.

B. Artificial Fault Experiment of Winding SC Faults

According to [11], [30], and [31], the ground and interturn SC winding faults are artificially simulated on the synchronous machine in this study. The experiments simulate the ground SC faults of different degrees by inserting a 40/20/10/0 Ω resistance at slot 1. The wiring diagram is shown in Fig. 5(a), and the typical IFRA curves are shown in Fig. 6(a). Windings in slots 1, 2, and 3 of the U-phase are SC to simulate different degrees of interturn SC faults. In addition, to obtain more data on different SC fault degrees, this study parallels the resistance values of 10 Ω to slots 1, 2, and 3, respectively, to simulate the change of fault degree. The simulated wiring diagram of interturn SC faults is shown in Fig. 5(b), and the typical IFRA curves are shown in Fig. 6(b). It can be seen in Fig. 6 that:

1) The IFRA curves of faulty winding are different from those of healthy winding, which makes it possible to detect and recognize the winding SC faults. The related references [17], [32], and [33] also detect winding faults by differences between frequency response curves.
2) The ground SC faults will cause the shift of the resonance point around 50 kHz to the HF band, and the smaller the resistance is, the more the IFRA curve deviates from the normal curve. The IFRA curves beyond 400 kHz, however, remain unchanged.
3) The interturn SC faults will also cause the shift of the resonance point around 50 kHz to the HF band. The variation of resonance is, however, not as significant as that of ground SC faults. What is more, the IFRA curves show a considerable variation in the range of

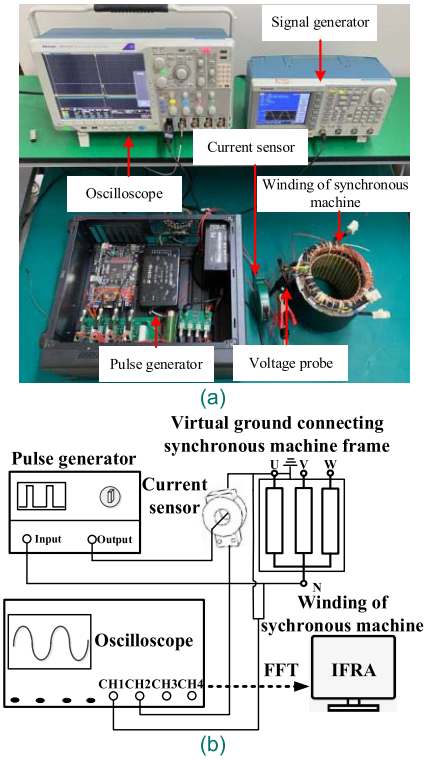

Fig. 3. Measurement experiment diagram of winding SC faults artificial simulation platform. (a) Actual wiring diagram. (b) Measurement wiring diagram.

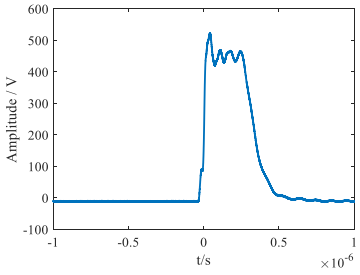

Fig. 4. Pulse waveform.

300–600 kHz, which is quite different from ground SC faults.

4) Under all fault situations, the faulty IFRA curves are similar to the normal curves at 600–1000 kHz. It shows that the two SC fault types have a limited impact on the HF band of frequency response. The HF band of IFRA is mainly dominated by equivalent capacitance, while the SC faults have an insignificant effect on equivalent capacitance [14].

The various winding SC faults of the synchronous machine are artificially stimulated, and an IFRA dataset is constructed. The dataset contains nine types. All fault types, degrees, and locations of machine winding SC faults are not included in this setup, but the most common fault type, namely, the ground and interturn SC faults, are included. This article aims to understand the mechanism of IFRA based on the image classification model. Thus, this setup is feasible and meaningful. There are 1808 sample data in the training set and 270 sample data in the test set. The details of the IFRA dataset are shown in Table II.

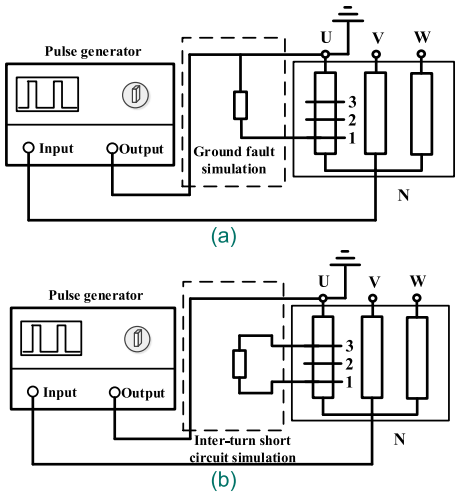

Fig. 5. Artificially simulated winding SC faults wiring diagram. (a) Simulated wiring diagram of ground SC faults. (b) Simulated wiring diagram of interturn SC faults.

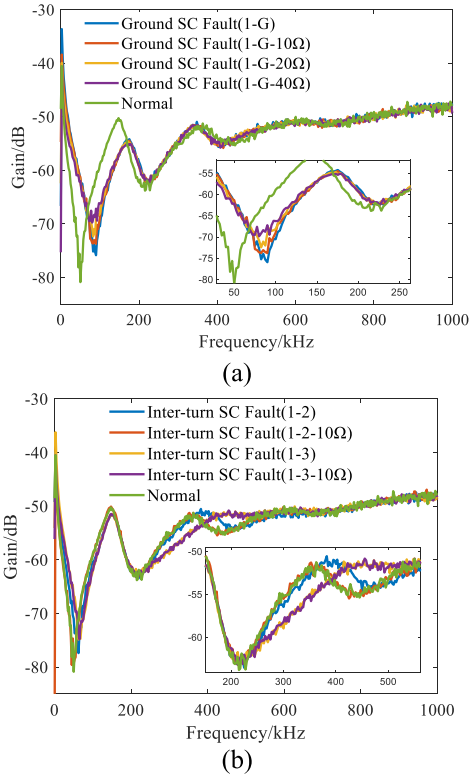

Fig. 6. IFRA curves of the synchronous machine in various winding fault states. (a) IFRA of ground SC faults in different degrees. (b) IFRA of interturn SC faults in different degrees.

IV. Establishment of Winding SC Faults Detection Model Based on Image Classification

A. Training Parameter Setting

Table III shows the configuration of the server when training image classification models. The loss function is cross-entropy, the mini-batch is 32, the epoch is 100, the optimizer is stochastic gradient descent (SGD), and the learning rate is 0.001.

TABLE II
IFRA DATASET OF THE SYNCHRONOUS MACHINE UNDER VARIOUS FAULT STATUSES

Type	Number of samples in the training set	Number of samples in the test set
Ground SC fault (1-G)	202	30
Ground SC fault (1-G-10Ω)	202	30
Ground SC fault (1-G-20Ω)	201	30
Ground SC fault(1-G-40Ω)	201	30
Inter-turn SC fault (1-2)	201	30
Inter-turn SC fault (1-2-10 Ω)	201	30
Inter-turn SC fault(1-3)	200	30
Inter-turn SC fault(1-3-10 Ω)	200	30
Normal	200	30

TABLE III
SERVER HARDWARE AND SOFTWARE CONFIGURATION

Device	Model
CPU	Inter(R) Xeon(R) Gold 6268CL × 2
GPU	NVIDIA RTX A4000
RAM	128G
SOFTWARE	Python
PACKAGE	Numpy, Pytorch, and torchcam

TABLE IV
STATISTICAL ACCURACY OF DIFFERENT IMAGE CLASSIFICATION MODELS

Type	Average accuracy(%)
Resnet18	99.63(99.25-100)
Resnet32	96.30(95.19-97.78)
Resnet50	94.07(92.60-96.30)
Resnet101	92.22(89.62-94.44)
Lenet	43.70 (40.74-44.44)
Alexnet	57.71(51.58-62.22)
Vgg	63.33(55.56-66.67)

B. Comparison of Different Image Classification Models

Deep learning methods for detecting machine winding SC faults based on image classification models are established and compared, and Table IV shows the average accuracy on the test set under 20 repeated experiments. Table IV shows that the average accuracy of Resnet18 is the highest, almost 100%, demonstrating its better performance than other networks. The reasons are as follows.

1) For large-scale Resnet, for instance, Resnet101, the training set has too few samples to update its parameters effectively, so the accuracy of the test set is reduced. Besides, there might be overfitting in large-scale Resnet, resulting in low accuracy in the test set.
2) Compared with different traditional datasets (Cifar-10, ImageNet, etc.), there is little difference between the IFRA curves of variable winding faults. Thus, Lenet is too simple to capture the various faults' feature information. The Alexnet and Vgg are less accurate than Resnet because the ability of this network to extract feature information is weaker than Resnet. On the other hand, gradient disappearance and explosion may be challenging to update the models'(except Resnet-based models) parameters effectively.

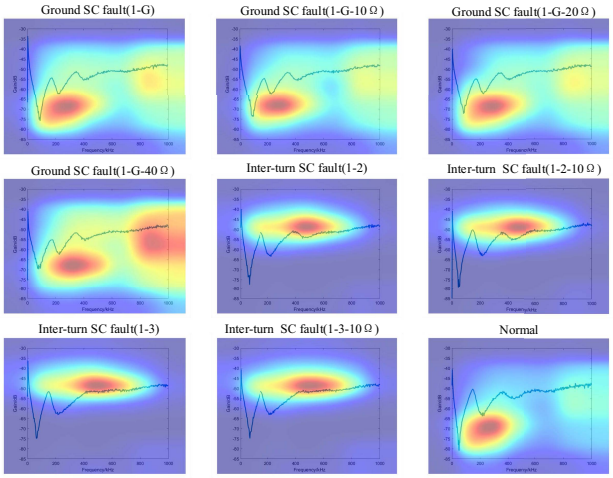

Fig. 7. Visualization results based on Resnet18 (99.63%) and Smooth Grad-CAM++ (To ensure the fairness of the comparison, all the experiments are carried out with the same samples, but the visualization results are universal).

3) According to the size of the IFRA dataset in this study, Resnet18 is more suitable. It will not have overfitting and underfitting caused by a too complex or simple structure.

V. IFRA DIFFERENCE ANALYSIS BASED ON SMOOTH GRAD-CAM++

A. Visualization Results Based on Resnet18 and Smooth Grad-CAM++

Fig. 7 shows the visualization results based on Resnet18 (test set accuracy: 99.63%) and Smooth Grad-CAM++. It can be seen in Fig. 7.

1) For ground SC faults, Resnet18 focuses on the IFRA curve from 1–400 kHz, and the HF band will also impact the classification process. It may be that the neural network focuses on the differences that the human eye does not [25]. The visualization result corresponds to the difference between IFRA curves of ground SC faults and normal winding, as shown in Fig. 6(a).
2) For interturn SC faults, it can be seen from Fig. 7 that the difference around 300–600 kHz between IFRA curves of interturn SC faults and normal winding is the largest, which also corresponds to Fig. 6(b).
3) For normal winding, its IFRA curve around the first resonance is different from that of other fault types, and it shows that the information of the first resonance point can be used to analyze the winding fault, which is also confirmed in [12].
4) According to the visualization results, as shown in Fig. 7, it can be demonstrated that the Resnet18 does extract the differences between variable frequency response curves and take it as the detection standard.

To illustrate the experiments' transparency, Fig. 8 shows visualization results based on Resnet18 (test set accuracy: 83.70%) and Smooth Grad-CAM++. It can be seen in Fig. 8 that Resnet18 cannot accurately capture the difference between frequency response curves when the accuracy is 83.70%. This indicates that the models' accuracy correlates positively with their feature information extraction capability.

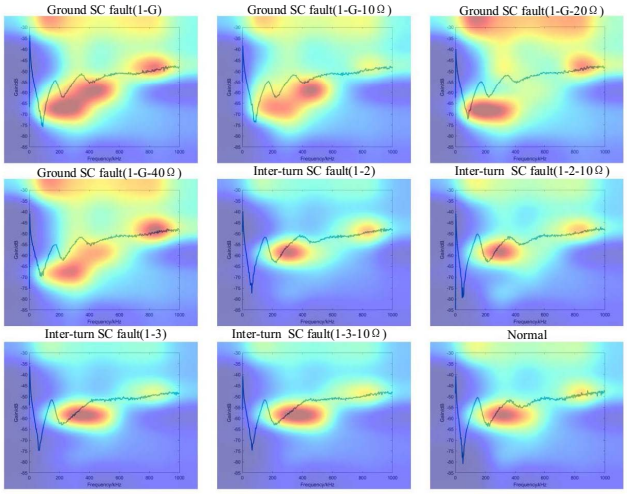

Fig. 8. Visualization results based on Resnet18 (83.70%) and Smooth Grad-CAM++.

TABLE V
CHINESE POWER INDUSTRY STANDARD DL/T 911

Deformation level	Limits for R_{XY}
Severe	R_{LF}<0.6
Moderate	1.0>R_{LF}≥0.6 or R_{MF}<0.6
Slight	2.0>R_{LF}≥1.0 or 0.6≤R_{MF}<1
Normal	R_{LF}≥2.0,R_{MF}≥1.0,and R_{HF}≥0.6
LF:1 kHz to 100kHz,MF:100kHz to 600kHz,HF:600kHz to 1MHz	

To further illustrate whether the visualization results of Smooth Grad-CAM++ are effective, the IFRA curve is analyzed quantitatively. This study uses the mathematical and statistical indicator, the relative coefficient R_{XY}, to analyze the faulty IFRA curves. The division of frequency band does not refer to this indicator's standard, the Chinese power industry standard DL/T 911 shown in Table V, but according to the results in Fig. 7: 1) for ground SC faults, the frequency range is divided into LF 1–400 kHz, MF 400–800 kHz, and HF 800–1000 kHz and 2) for interturn SC faults, the frequency range is divided into LF 1–300 kHz, MF 300–600 kHz, and HF 600–1000 kHz. The R_{XY} is calculated as follows (12)–(15), as shown at the bottom of the next page, where X_i and Y_i are the ith elements of the measured normal IFRA and measured IFRA of different faults, respectively, and N is the number of elements. The smaller the R_{XY} is, the more severe fault is.

Table VI shows the R_{xy} of all winding SC faults based on original DL/T 911 [12], and all states are detected by Table V. Tables VII and VIII show the R_{XY} and states of ground and interturn SC faults in different degrees according to new frequency bands with DL/T 911. From Tables VI to VIII, it can be seen that,

1) If the original DL/T911 standard is used to detect the relevant IFRA data, there are two obvious errors in Table VI. The first one is that all ground SC faults are moderate, while the real SC faults are devastating to the machines [1] and should be severe. The second is that the interturn SC fault (1–2–10 Ω) is detected as normal.

TABLE VI
R_{xy} AND STATE ACCORDING TO DL/T 911

Type (kHz)	1-100	100-600	600-1000	State (based on Tab V)
Ground SC fault (1-G)	1.5268	0.5511	0.8641	Moderate ✗
Ground SC fault (1-G-10Ω)	1.1457	0.5613	0.9251	Moderate ✗
Ground SC fault (1-G-20Ω)	1.1743	0.5639	0.8000	Moderate ✗
Ground SC fault (1-G-40Ω)	1.3155	0.5765	0.8749	Moderate ✗
Inter-turn SC fault (1-2)	1.9234	0.9659	0.8782	Slight
Inter-turn SC fault (1-2-10Ω)	3.1634	1.7706	0.8817	Normal✗
Inter-turn SC fault (1-3)	1.7757	0.6881	0.8463	Slight
Inter-turn SC fault (1-3-10Ω)	1.5075	0.6852	0.8856	Slight

TABLE VII
R_{xy} OF GROUND SC FAULTS IN DIFFERENT DEGREES ACCORDING TO NEW FREQUENCY BANDS

Type (kHz)	**1-400**	400-800	800-1000	State (based on Tab V)
Ground SC fault (1-G)	**0.5144**	0.5511	0.8641	Severe↑
Ground SC fault (1-G-10Ω)	**0.5267**	0.5613	0.9251	Severe↑
Ground SC fault (1-G-20Ω)	**0.5518**	0.5639	0.8000	Severe↑
Ground SC fault (1-G-40Ω)	**0.5631**	0.5765	0.8749	Severe↑

TABLE VIII
R_{xy} OF INTERTURN SC FAULTS IN DIFFERENT DEGREES ACCORDING TO NEW FREQUENCY BANDS

Type (kHz)	1-300	**300-600**	600-1000	State (based on Tab V)
Inter-turn SC fault (1-2Ω)	1.5551	**0.2745**	0.8782	Moderate↑
Inter-turn SC fault (1-2-10Ω)	2.6324	**0.9052**	0.8817	Slight↑
Inter-turn SC fault (1-3)	1.0448	**0.1164**	0.8463	Moderate↑
Inter-turn SC fault (1-3-10Ω)	1.2714	**0.1173**	0.8856	Moderate↑

2) But when the frequency bands obtained from the visualization results are used, the reliability of the diagnosis is significantly improved in Tables VII and VIII.
3) The most significant difference between IFRA curves of all winding states corresponds to the visualization results of Fig. 7 based on Smooth Grad-CAM++. In addition, it also shows that the trained Resnet18 is very effective.
4) We give some effective suggestions based on the above results. Although it may not apply to all machines, it may apply to machines of the same type as the experimental objects in this study. If one wants to detect the ground SC faults, more attention should be paid to 1–400 kHz. A similar suggestion may be extended to interturn SC fault, but the frequency band changes to 300–600 kHz.

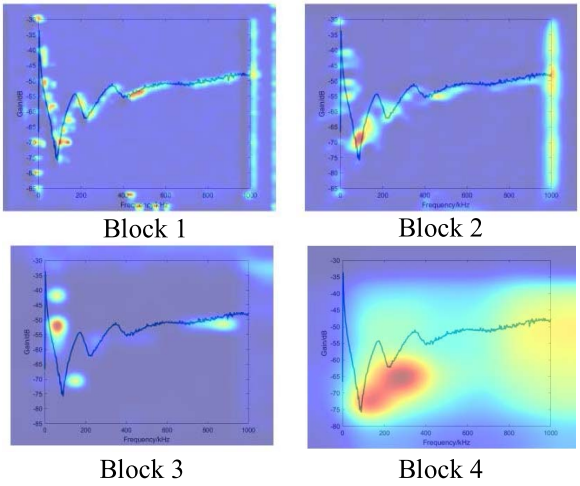

Fig. 9. Visualization results using Resnet18 under different blocks.

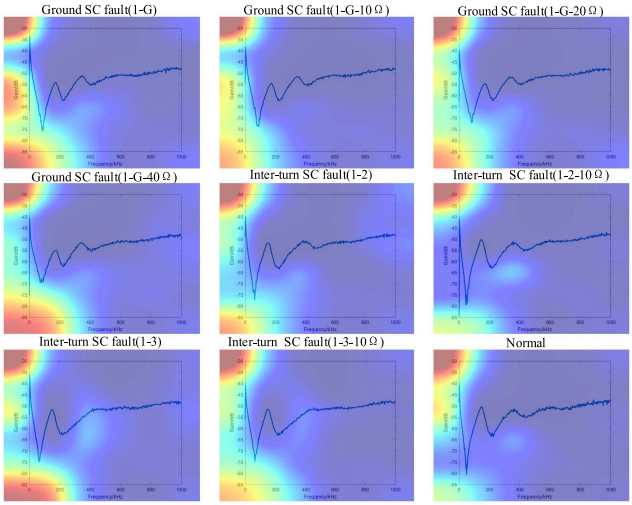

Fig. 10. Visualization results based on Alexnet and Smooth Grad-CAM++.

In addition, we can get the visualization results of different convolution layers based on Smooth Grad-CAM++. The Resnet18 has four blocks. Fig. 9 shows the visualization results under different blocks. It shows that the more layers behind, the more classification details captured by the convolution layer, so the clearer the visualization result of Smooth Grad-CAM++.

B. Visualization Results of Other Image Classification Models

The visualization results based on Smooth Grad-CAM++ can also be used to explain the poor performance of some other image classification models. This study takes Alexnet as an example, and Fig. 10 shows the visualization results based on Alexnet. It can be seen from Fig. 10 that Alexnet pays attention to the LF range. The most significant difference of IFRA is, however, around 300–600 kHz for interturn SC faults, which shows that the low classification accuracy of Alexnet is due to the failure to extract the feature information of interturn SC faults.

C. Selection of Coordinate and Frequency Band

Many researchers [17], [33] believe that the changes of IFRA at the LF band are noticeable, caused by some fault types that undoubtedly change the equivalent inductance of winding. Thus, IFRA in logarithmic coordinate is often used to analyze winding faults. This study also uses the IFRA dataset in logarithmic coordinates to train Resnet18. It is found that the accuracy of the test set is 89.63%, which does not achieve the expectation. The Smooth Grad-CAM++ is also used to visualize the trained Resnet18, as shown in Fig. 11. As can be seen in Fig. 11, the low accuracy of Resnet18 is due to the fact that the frequency range (300–600 kHz) with significant differences is compressed and logarithmic coordinate makes network focus more on 1–100 kHz with slight differences. Thus, to better detect winding faults when using image classification models, a linear coordinate of IFRA is suggested.

In addition, as mentioned in the introduction, the current diagnosis of synchronous machines refers to the FRA standard of power transformers [11], [12]. Thus, some researchers [12], [32], [33] directly use a frequency band of 1–1000 kHz to detect synchronous machine winding SC faults but do not provide the corresponding experimental analysis and basis (results in Table IV also are obtained by this frequency range). Here, the models' average accuracy, training time (time required to train a model), and detection time (time required to detect the test set) are used to explain this issue. Table IX shows the average accuracy, training time, and detection time

$$D_X = \frac{1}{N}\sum_{i=1}^{N}\left(X_i - \frac{1}{N}\sum_{i=1}^{N}X_i\right)^2 \tag{12}$$

$$D_Y = \frac{1}{N}\sum_{i=1}^{N}\left(Y_i - \frac{1}{N}\sum_{i=1}^{N}Y_i\right)^2 \tag{13}$$

$$P_{XY} = \frac{\frac{1}{N}\sum_{i=1}^{N}\left(X_i - \frac{1}{N}\sum_{i=1}^{N}X_i\right)\sum_{i=1}^{N}\left(Y_i - \frac{1}{N}\sum_{i=1}^{N}Y_i\right)^2}{\sqrt{D_X D_Y}} \tag{14}$$

$$R_{XY} = \begin{cases} 10, & 1 - P_{XY} < 10 \\ -\log_{10}(1 - P_{XY}), & \text{otherwise} \end{cases} \tag{15}$$

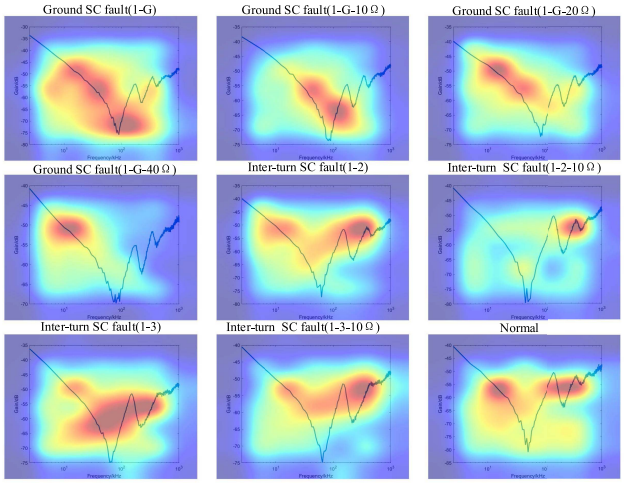

Fig. 11. Resnet18 visualization results in logarithmic coordinates.

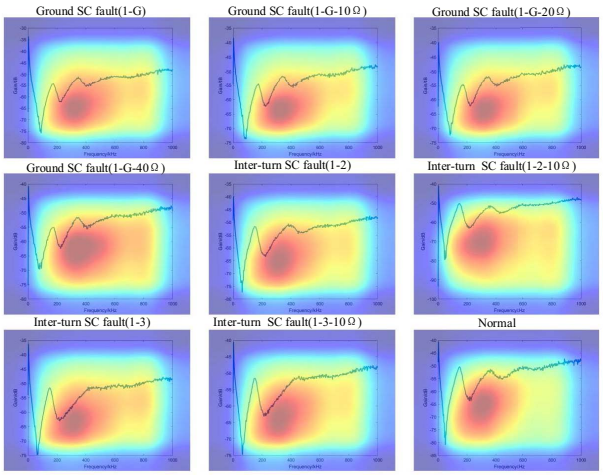

Fig. 12. Visualization results based on Resnet18 and CAM.

TABLE IX
ACCURACY OF RESNET18 IN DIFFERENT FREQUENCY RANGES

Frequency range (kHz)	100-200	200-600	100-600	1-600	1-1000
Average accuracy (%)	66.30	93.70	97.78	99.5	99.63
Training time (min)	13.3	17.3	18.4	20.9	26.5
Detection time (s)	23	27	31	35	37

of Resnet18 using different frequency ranges. It can be seen in Table IX that,

1) Using an IFRA of 1–1000 kHz does not have certain advantages, and it needs extra time, although its average accuracy is higher than that in other frequency ranges.
2) If the frequency range of 1–600 kHz is used, the amount of calculation can be reduced on the premise of maintaining the model's accuracy, which also corresponds to the visualization results in Fig. 7.

D. Comparison of Different Interpretability Models

Fig. 12 shows the visualization results under the interpretability model CAM. Compared to the visualization results in Fig. 7, the results in Fig. 12 appear to have no focus. This is because the CAM is only a sensitivity analysis of a single output, as shown in (4), without considering the surrounding outputs.

VI. CASE STUDY

The machine involved in the case study is an 8 kW synchronous machine, as shown in Fig. 13. The frequency response curves in the ground and interturn SC fault, shown in Fig. 14, are obtained using the same experimental setup in Section III. Table X is R_{xy} of winding SC faults based on the original DL/T 911. Tables XI and XII show the R_{xy} and states of ground and interturn SC faults according to new frequency bands. Fig. 14 and Tables XI and XII show that the suggestions (using new frequency bands) given in this study are generalized for similar synchronous machines, and some conclusions (change of the first resonance point) are reproducible.

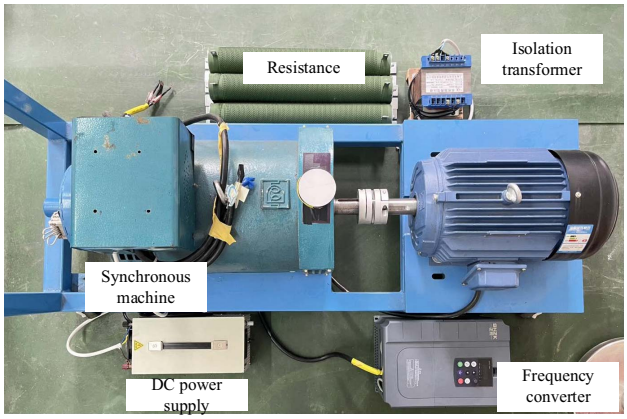

Fig. 13. 8 kW synchronous machine physical diagram.

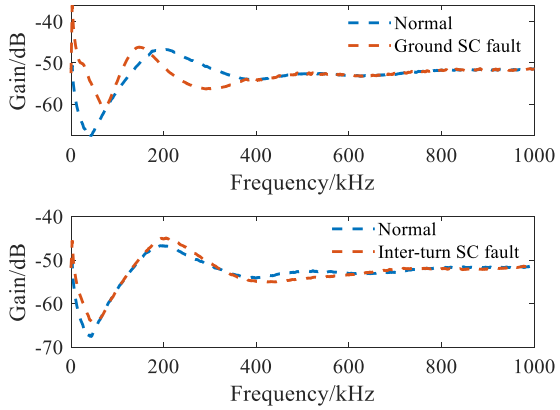

Fig. 14. IFRA curves of the 8 kW synchronous machine in ground SC fault and interturn SC fault.

VII. DISCUSSION

The proposed conclusions differ from previous related studies [11], [12], [15], [16], [17] based on the FRA standard of power transformers, for instance, using linear coordinates and changing the subfrequency bands to calculate the mathematical and statistical indicator. Synchronous machines and transformers have more significant differences in structure and operating environment, so it is acceptable to use a different standard.

TABLE X
R_{xy} AND STATE ACCORDING TO DL/T 911 UNDER 8 kW MACHINE

Type (kHz)	1-100	100-600	600-1000	State (based on Tab V)
Ground SC fault	0.6507	0.1219	1.6786	Moderate
Inter-turn SC fault	1.002	1.8356	0.6817	Slight

TABLE XI
R_{xy} OF GROUND SC FAULTS ACCORDING TO NEW FREQUENCY BANDS

Type (kHz)	**1-400**	400-800	800-1000	State (based on Tab V)
Ground SC fault	**0.0887**	1.9781	1.6381	Severe↑

TABLE XII
R_{xy} OF GROUND SC FAULTS ACCORDING TO NEW FREQUENCY BANDS

Type (kHz)	1-300	**300-600**	600-1000	State (based on Tab V)
Inter-turn SC fault	1.3826	**0.5943**	0.6817	Moderate↑

The differences in IFRA curves in Fig. 6 seems relatively small; however, in the subfrequency bands, there are indeed some differences (1–400 kHz for ground SC faults, 300–600 kHz for interturn SC faults). It may be challenging to observe these differences visually, but the proposed method based on deep learning provides objective visualization results of the difference, and it shows that the deep learning-based diagnosis process is based on those differences to detect the relevant faults. According to visualization results, this study provides suggestions for diagnosing synchronous machine winding SC faults by frequency response, which corresponds to the previous works, but there are subtle differences in the data processing.

In Section V, we change the relevant frequency bands based on the visualization results, which obviously improved the accuracy of using the mathematical and statistical indicator to detect the severity of synchronous machine winding SC faults. Thus, before detecting the winding faults, the relevant visualization results and new subfrequency bands can be analyzed according to the proposed method if the fault dataset is obtained by precision modeling and true-type experiments, which could increase the performance of the diagnosis method.

In Section VI, we use a case study of an 8 kW synchronous machine to illustrate that our proposed suggestions are informative for similar machines. Perhaps the derived conclusions in this study only correspond to the same type of machine as the experimental machine because of data insufficiency. This article, however, provides a general method to understand the detection mechanism of the IFRA method, which is beneficial for researchers to have a more objective interpretation of the frequency response curve for their machines.

VIII. CONCLUSION

This study proposes a method to visualize, analyze, and understand the mechanism of IFRA for detecting synchronous machine winding SC faults based on the image classification model and Smooth Grad-CAM++. According to the experimental results, the following conclusions are drawn.

1) According to the accuracy comparison results of the different typical image classification models, when using the image classification method to detect synchronous machines' winding SC faults, if the dataset is small, Resnet18 can be used. The accuracy of this network is high, which are easy to prevent underfitting and overfitting.
2) According to the results of the visualization experiment, the following more general suggestions are provided for synchronous machines of the same type as the test object in this study. When detecting SC faults based on IFRA, the ground SC fault should focus on the LF band, while the interturn SC fault can concentrate on the MF band of IFRA, respectively. It is suggested to use IFRA with linear coordinates to detect SC faults when the image classification method is used, which can better capture the MF and HF oscillation areas. The first resonance point of the IFRA curve can be given special and careful attention for detecting winding SC faults.
3) There is no need to use the information of the entire 1–1000 kHz, while the amount of calculation can be reduced with particular frequency bands.
4) By changing subfrequency bands of frequency response based on visualization results of Smooth Grad-CAM++, the diagnosis performance of the statistical indicator based on new subfrequency bands is improved compared with that based on the original DL/T 911 standard.
5) The proposed method can guide the models' training process and data collection and be used to judge whether the models pay attention to the IFRA's feature information and improve the models' reliability. In the future, more diverse IFRA datasets will be produced, enabling interpretability models to be applied to various synchronous machines.

REFERENCES

[1] I.-H. Kao, W.-J. Wang, Y.-H. Lai, and J.-W. Perng, "Analysis of permanent magnet synchronous motor fault diagnosis based on learning," *IEEE Trans. Instrum. Meas.*, vol. 68, no. 2, pp. 310–324, Feb. 2019.
[2] S. Du, J. Hu, Y. Zhu, and M. Zhang, "An improved displacement measurement based on model reconstruction for permanent magnet synchronous motor," *IEEE Trans. Instrum. Meas.*, vol. 66, no. 11, pp. 3044–3051, Nov. 2017.
[3] H. A. Toliyat, S. Nandi, and S. Choi, *Electric Machines: Modeling, Condition Monitoring and Fault Diagnosis*. Boca Raton, FL, USA: CRC Press, 2012.
[4] K. N. Gyftakis and A. J. Marques-Cardoso, "Reliable detection of very low severity level stator inter-turn faults in induction motors," in *Proc. IECON 45th Annu. Conf. IEEE Ind. Electron. Soc.*, Oct. 2019, pp. 1290–1295.
[5] Z. D. Jia et al., "Modeling simulation and diagnosis analysis of inter-turn short circuits fault in generator rotor," *High Voltage Eng.*, vol. 45, no. 12, pp. 3932–3940, 2019.
[6] T. Li et al., "Simulation study on interturn short circuit of rotor windings in generator by RSO method," in *Proc. IEEE Int. Conf. High Voltage Eng. Appl. (ICHVE)*, Sep. 2018, pp. 1–4.
[7] G.-A. Capolino and A. Cavagnino, "New trends in electrical machines technology—Part II," *IEEE Trans. Ind. Electron.*, vol. 61, no. 9, pp. 4931–4936, Sep. 2014.
[8] C. Bruzzese, "Diagnosis of eccentric rotor in synchronous machines by analysis of split-phase currents—Part II: Experimental analysis," *IEEE Trans. Ind. Electron.*, vol. 61, no. 8, pp. 4206–4216, Aug. 2014.

[9] W. Shuting, L. Yonggang, L. Heming, and T. Guiji, "The new diagnosis method of rotor winding inter-turn short circuit fault and imbalance fault based on stator and rotor vibration characteristics," in *Proc. Int. Conf. Electr. Mach. Syst.*, Sep. 2005, pp. 2207–2210.
[10] X. Huang, Q. Tan, L. Li, J. Li, and Z. Qian, "Winding temperature field model considering void ratio and temperature rise of a permanent-magnet synchronous motor with high current density," *IEEE Trans. Ind. Electron.*, vol. 64, no. 3, pp. 2168–2177, Mar. 2017.
[11] Y. Chen et al., "Fault anomaly detection of synchronous machine winding based on isolation forest and impulse frequency response analysis," *Measurement*, vol. 188, Jul. 2022, Art. no. 110531.
[12] Z. Zhao, Y. Chen, Y. Yu, M. Han, C. Tang, and C. Yao, "Equivalent broadband electrical circuit of synchronous machine winding for frequency response analysis based on gray box model," *IEEE Trans. Energy Convers.*, vol. 36, no. 4, pp. 3512–3521, Dec. 2021.
[13] S. Wang, S. Wang, H. Feng, Z. Guo, S. Wang, and H. Li, "A new interpretation of FRA results by sensitivity analysis method of two FRA measurement connection ways," *IEEE Trans. Magn.*, vol. 54, no. 3, pp. 1–4, Mar. 2018.
[14] V. Nurmanova, M. Bagheri, A. Zollanvari, K. Aliakhmet, Y. Akhmetov, and G. Gharehpetian, "A new transformer FRA measurement technique to reach smart interpretation for inter-disk faults," *IEEE Trans. Power Del.*, vol. 34, no. 4, pp. 1508–1519, Aug. 2019.
[15] X. Mao, Z. Wang, Z. Wang, and P. Jarman, "Accurate estimating algorithm of transfer function for transformer FRA diagnosis," in *Proc. IEEE Power Energy Soc. Gen. Meeting (PESGM)*, Aug. 2018, pp. 1–5.
[16] N. Hashemnia, A. Abu-Siada, and S. Islam, "Improved power transformer winding fault detection using FRA diagnostics—Part 1: Axial displacement simulation," *IEEE Trans. Dielectr. Electr. Insul.*, vol. 22, no. 1, pp. 556–563, Feb. 2015.
[17] A. Mugarra, C. A. Platero, J. A. Martínez, and U. Albizuri-Txurruka, "Validity of frequency response analysis (FRA) for diagnosing large salient poles of synchronouos machines," *IEEE Trans. Ind. Appl.*, vol. 56, no. 1, pp. 226–234, Feb. 2020.
[18] J. Ni, Z. Zhao, S. Tan, Y. Chen, C. Yao, and C. Tang, "The actual measurement and analysis of transformer winding deformation fault degrees by FRA using mathematical indicators," *Electr. Power Syst. Res.*, vol. 184, Jul. 2020, Art. no. 106324.
[19] J. Liu, Z. Zhao, C. Tang, C. Yao, C. Li, and S. Islam, "Classifying transformer winding deformation fault types and degrees using FRA based on support vector machine," *IEEE Access*, vol. 7, pp. 112494–112504, 2019.
[20] J. Liu, Z. Zhao, K. Pang, D. Wang, C. Tang, and C. Yao, "Improved winding mechanical fault type classification methods based on polar plots and multiple support vector machines," *IEEE Access*, vol. 8, pp. 216271–216282, 2020.
[21] Y. Luo, J. Qiu, and C. Shi, "Fault detection of permanent magnet synchronous motor based on deep learning method," in *Proc. 21st Int. Conf. Electr. Mach. Syst. (ICEMS)*, Oct. 2018, pp. 699–703.
[22] C. F. Chen, O. Li, C. F. Tao, A. J. Barnett, J. Su, and C. Rudin, "This looks like that: Deep learning for interpretable image recognition," in *Proc. 33rd Conf. Neural Inf. Process. Syst. (NeurIPS)*, vol. 32, Vancouver, BC, Canada, 2019, pp. 8930–8941.
[23] S. Hooker, D. Erhan, P. J. Kindermans, and B. Kim, "A benchmark for interpretability methods in deep neural networks," in *Proc. 33rd Conf. Neural Inf. Process. Syst. (NeurIPS)*, vol. 32, Vancouver, BC, Canada, 2019, 2019, pp. 9737–9748.
[24] T. Miller, "Explanation in artificial intelligence: Insights from the social sciences," *Artif. Intell.*, vol. 267, pp. 1–38, Feb. 2019.
[25] R. Zellers, Y. Bisk, A. Farhadi, and Y. Choi, "From recognition to cognition: Visual commonsense reasoning," in *Proc. IEEE/CVF Conf. Comput. Vis. Pattern Recognit. (CVPR)*, Jun. 2019, pp. 6713–6724.
[26] H. Yang, X. Li, and W. Zhang, "Interpretability of deep convolutional neural networks on rolling bearing fault diagnosis," *Meas. Sci. Technol.*, vol. 33, no. 5, May 2022, Art. no. 055005.
[27] Z. Fan, X. Xu, R. Wang, and H. Wang, "Fan fault diagnosis based on lightweight multiscale multiattention feature fusion network," *IEEE Trans. Ind. Informat.*, vol. 18, no. 7, pp. 4542–4554, Jul. 2022.
[28] B. Zhou, A. Khosla, A. Lapedriza, A. Oliva, and A. Torralba, "Learning deep features for discriminative localization," in *Proc. IEEE Conf. Comput. Vis. Pattern Recognit. (CVPR)*, Jun. 2016, pp. 2921–2929.
[29] D. Omeiza, S. Speakman, and C. Cintas, "Smooth Grad-CAM++: An enhanced inference level visualization technique for deep convolutional neural network models," 2019, *arXiv:1908.01224*.
[30] X. Liu, W. Miao, Q. Xu, L. Cao, C. Liu, and P. W. T. Pong, "Inter-turn short-circuit fault detection approach for permanent magnet synchronous machines through stray magnetic field sensing," *IEEE Sensors J.*, vol. 19, no. 18, pp. 7884–7895, Sep. 2019.
[31] A. Mohammed, J. I. Melecio, and S. Djurović, "Open-circuit fault detection in stranded PMSM windings using embedded FBG thermal sensors," *IEEE Sensors J.*, vol. 19, no. 9, pp. 3358–3367, May 2019.
[32] Y. Yu, Z. Zhao, Y. Chen, H. Wu, C. Tang, and W. Gu, "Evaluation of the applicability of IFRA for short circuit fault detection of stator windings in synchronous machines," *IEEE Trans. Instrum. Meas.*, vol. 71, pp. 1–12, 2022.
[33] F. R. Blánquez, C. A. Platero, E. Rebollo, and F. Blázquez, "Field-winding fault detection in synchronous machines with static excitation through frequency response analysis," *Int. J. Elect. Power Energy Syst.*, vol. 73, pp. 229–239, Dec. 2015.

Yu Chen was born in Wenzhou, Zhejiang, China, in 2000. He received the B.S. degree from the College of Engineering and Technology, Southwest University, Chongqing, China, in 2022. He is currently pursuing the master's degree with the School of Electrical and Electronic Engineering, Huazhong University of Science and Technology, Wuhan, Hubei.

His current research interests include condition monitoring, fault diagnosing for power equipment, and the application of artificial intelligence.

Zhongyong Zhao (Member, IEEE) was born in Guangyuan, Sichuan, China. He received the B.S. and Ph.D. degrees in electrical engineering from Chongqing University, Chongqing, China, in 2011 and 2017, respectively.

He received a Scholarship from the China Scholarship Council to enable him to attend a Joint-Training Ph.D. Program in Curtin University, Perth, WA, Australia, from 2015 to 2016. He is currently an Associate Professor with the College of Engineering and Technology, Southwest University, Chongqing. His current research interests include condition monitoring and fault diagnosing for HV apparatus and artificial intelligence.

Yueqiang Yu was born in Nanchong, Sichuan, China, in 1994. He received the B.S. degree from the Chongqing University of Science and Technology, Chongqing, China, in 2017. He is currently pursuing the master's degree with the Department of Electrical Engineering, College of Engineering and Technology, Southwest University, Chongqing.

His current research interests include condition monitoring and fault diagnosing of machines.

Wei Wang was born in Shaoyang, Hunan, China, in 1998. He received the B.S. degree from the School of Electrical and Information Engineering, Changsha University of Science and Technology, Changsha, China, in 2019. He is pursuing the Ph.D. degree with the School of Electrical and Electronic Engineering, Huazhong University of Science and Technology, Wuhan, Hubei, China.

His current research interests include proton therapy, medical physics, and the application of deep learning.

Chao Tang (Member, IEEE) was born in Sichuan, China, in 1981. He received the M.S. and Ph.D. degrees in electrical engineering from Chongqing University, Chongqing, China, in 2007 and 2010, respectively.

As a Ph.D. Student from 2008 to 2009 and as a Visiting Scholar from 2013 to 2013 and 2015 to 2016, he studied with the Tony Davies High Voltage Laboratory, University of Southampton, U.K., doing some research on the dielectric response characteristics and space charge behaviors of oil-paper insulation. He is currently a Professor with the College of Engineering Technology, Southwest University, Chongqing. His current research interests include mainly in the field of online monitoring of insulation conditions and fault diagnosis for high-voltage equipment.